PAPER 2

Submitted for publication in *Journal of Solid State Chemistry*

Crystal structure and magnetic properties of $La_2Co_2O_5$

Ole H. Hansteen[a], Helmer Fjellvåg[a] and Bjørn C. Hauback[b]

[a] *Department of Chemistry, University of Oslo, N-0315 Oslo, Norway*

[b] *Institutt for energiteknikk, N-2007 Kjeller, Norway*

ABSTRACT

The crystal structure of $La_2Co_2O_5$ is determined on the basis of high resolution powder X-ray diffraction and neutron diffraction data. $La_2Co_2O_5$ adopts the brownmillerite type structure where single layers of corner-sharing CoO_6-octahdra are connected by layers with chains of corner-sharing CoO_4-tetrahedra running along [100]. Three alternative descriptions of the crystal structure in space groups *Pnma*, *Imma* and *Ima2* with slightly different structural distortions and/or atomic disorder, are discussed. The unit cell is; a = 544.45 (2) pm, b = 1586.89 (4) pm, c = 569.22 (2) pm; R_{wp}(PXD) = 8.0%, R_{wp}(PND) = 7.3%, R_p(PXD) = 5.3%, R_p(PND) = 5.6% (space group *Pnma*). On reducing $LaCoO_3$ to $La_2Co_2O_5$ there is a 9.8 % expansion of the unit cell owing to the increased size of high-spin divalent cobalt atoms, and a significant peak broadening occurs in the high resolution PXD data. On the basis of powder neutron diffraction data, $La_2Co_2O_5$ is found to order antiferromagnetically (G-type ordering) for temperatures below $T_N = 301 \pm 5$ K. The magnetic moments for the cobalt atoms are $\mu_{oct.} = 3.0 \pm 0.1\mu_B$ and $\mu_{tetr.} = 2.5 \pm 0.1\mu_B$.

INTRODUCTION

Anion vacancy ordering is common for oxygen deficient perovskites ($AMO_{3-\delta}$), and results in superstructures where the cationic sublattice of the perovskite is left essentially unchanged. The coordination of some or all the M atoms, which usually is a transition element, decreases from octahedral to typically square pyramidal, tetrahedral or square planar, e.g. $Ca_2Mn_2O_5$ (1), $Ca_2Fe_2O_5$ (2), and $La_2Ni_2O_5$ (3), respectively. The type of vacancy ordering is strongly dependent on the nature of the transition element. $A_2M_2O_5$ compounds with tetrahedral coordination of M often adopt the brownmillerite type structure. Here the anion vacancy ordering leads to the formation of layers with chains of corner-sharing MO_4-tetrahedra connecting single perovskite layers of corner-sharing MO_6-octahedra.

Reduction of perovskite type oxides leads to loss of oxygen, which in most cases is connected with formation of oxygen vacancies. At low vacancy consentrations clustering occurs, whereas at higher consentrations ordered phases are normally formed. Vidyasagar *et al.* (3) showed that reduction of $LaCoO_3$ at low temperatures lead to the ordered phase $La_2Co_2O_5$ for which the brownmillerite type structure was proposed. The lowering of valence state of cobalt from three to two, is expected to give rise to considerably different electronic and magnetic properties. The present study reports on a detailed determination of the crystal and magnetic structure of $La_2Co_2O_5$ based on a combined profile analysis of high resolution powder X-ray diffraction data collected at ESRF and powder neutron diffraction data.

EXPERIMENTAL

Synthesis. $La_2Co_2O_5$ was prepared by isothermal reduction of single phase $LaCoO_3$. $LaCoO_3$ was first prepared by a citrate precursor method (4). The starting materials for the synthesis were La_2O_3 (99.99% Molycorp), $Co(CH_3COO)_2{\cdot}4H_2O$ (>99% Fluka) and citric acid monohydrate, $C_3H_4(OH)(COOH)_3{\cdot}H_2O$ (>99.8% Riedel-de Haën). Single phase $LaCoO_3$ was obtained after calcination of the precursor powder in air at 1300 K for 110 hours with two intermediate grindings followed by repelletization. Phase purity was assured from powder X-ray diffraction. The isothermal reduction of $LaCoO_3$ to $La_2Co_2O_5$ was performed in sealed silica glass ampoules using chips of Zr (99.5% A. D. Mackay Inc.) as reducing agent (oxygen getter). The ampoules with the samples inside, were repeatedly flushed with argon before evacuation and sealing in order to minimize the amount of gaseous oxygen in the system prior to the reduction. The sample was held in an alumina crucible at 673 K, and was separated (by approximately 160 mm) from the Zr, which was positioned in the warmer zone of the furnace at 873 K in order to assure complete oxidation to ZrO_2 (5). After reaction and equilibration for

seven days, all samples were cooled in ice-water. The ampoules were opened in an argon filled glovebox [$p(O_2)$ and $p(H_2O) < 1$ ppm]. Care was taken to assure inert atmosphere during storage, handling and subsequent characterization of specimens.

Powder diffraction. Room temperature powder X-ray diffraction (PXD) data were collected for all samples with a Guinier Hägg camera using Si as internal standard (a = 543.1065 pm). The sample holders were filled with oil and sealed with Scotch tape on top and bottom. The sample adhered to the bottom tape which prevented it from dispersing into the oil. Both Cr$K\alpha_1$ [detection limit for impurities ca. 0.3 wt% (6)] and Cu$K\alpha_1$ radiation were used. Unit cell dimensions were determined by least squares calculations using the program UNITCELL (7). Synchrotron (SR) PXD data were collected for $La_2Co_2O_5$ with the powder diffractometer in Debye-Scherrer mode at the Swiss Norwegian Beam Line (BM1) at ESRF (Grenoble). Monochromatic X-rays of wavelength 109.803 pm were obtained from a channel-cut Si(111) crystal. The sample was contained in a sealed and rotating glass capillary with diameter 0.2 mm (chosen for reducing absorption). Intensity data were collected at 298 K between $2\theta = 3.5$ and 63° in steps of $\Delta(2\theta) = 0.008°$. Powder neutron diffraction (PND) data were collected for $La_2Co_2O_5$ with the two-axis powder diffractometer OPUS at the JEEP II reactor, Kjeller (Norway). A cylindrical sample holder of aluminum, carefully sealed with an indium washer, was used. Monochromatized neutrons of wavelength 182.5 pm were obtained by reflection from Ge(111). The scattered intensities were measured by five ^{3}He detectors positioned 10° apart. Intensity data were collected at 10 K and 298 K between $2\theta = 7$ and 102° in steps of $\Delta(2\theta) = 0.05°$. The GSAS program package (8) was used for the combined Rietveld-type profile refinements of powder synchrotron X-ray and neutron diffraction data collected at 298 K. Table 1 summarizes the characteristic features of the data sets and the variable parameters entering the least-squares refinements. The initial structural model of brownmillerite type was based on the description of orthorhombic $Ca_2Fe_2O_5$, space group *Pnma* (2). For the synchrotron PXD data the background was modelled by a power series in $Q^{2n}/n!$ and $n!/Q^{2n}$ where $Q = 2\pi/d$ (GSAS function #6). The peak shape was modelled by a pseudo-Voigt function using three Gaussian half width parameters (U, V, W) and three Lorentzian coefficients (two Scherrer broadening coefficients and one strain broadening coefficient). For the PND data the background was modelled by cosine Fourier series polynomials, and the peak shape was modelled by a Gaussian function. The scattering lengths $b_{La} = 8.27$ fm, $b_{Co} = 2.53$ fm and $b_O = 5.81$ fm were taken from the GSAS library. For profile

TABLE 1 Characteristic features of the powder synchrotron X-ray (298 K) and neutron diffraction (10, 298 K) data sets for $La_2Co_2O_5$, and list of parameters entering the profile refinements.

	PXD(SR)				PND	
Measured data points	7424				1764	
Reflections (hkl)	244				178	
λ (pm)	109.803				182.5	
Scale factor	1				1	
Zero point	1				1	
Profile parameters	6				3	
Unit cell dimensions			3[a]			
Positional parameters			13[a]			
Isotropic displacement factors			3[a]			
Magnetic components					(4)[b]	
Background coefficients	15				12	
Refinable parameters	23	+	19	+	17	= 59

[a] Common parameters for PXD(SR) and PND in the combined refinements.
[b] Only refined for the 10 K data.

refinement of the PND data collected at 10 K (crystal and magnetic structure) the Hewat version (9) of the Rietveld program (10) was used.

Magnetic measurements. Magnetic susceptibility data were measured by a Quantum Design SQUID-magnetometer (MPMS) in the temperature range 2 - 300 K for magnetic fields (H) up to 40.0 kOe. All samples were zero field cooled and the temperature dependence of the magnetic susceptibility was measured on heating. A Faraday balance was used for susceptibility measurements performed on heating in the temperature range 300 - 970 K; $H \leq 7.0$ kOe. The samples were held in evacuated and sealed spherical silica glass ampoules. The measured magnetic susceptibility was corrected for diamagnetic contribution from the sample container and from core electrons.

RESULTS AND DISCUSSION

(i) Crystal structure.

The Guinier-Hägg PXD pattern at 298 K for $La_2Co_2O_5$ was indexed satisfactorily using the primitive orthorhombic unit cell description of a brownmillerite type crystal structure. The description by Berggren (2) for orthorhombic $Ca_2Fe_2O_5$ (space group *Pnma*) was used as starting model for the combined Rietveld type refinements of the synchrotron PXD and the

PND data. The results are given in Tables 2 - 4. The unit cell dimensions are somewhat lower than reported by K. Vidyasagar *et al.* (3). The crystal structure, Fig. 1, is a layered arrangement consisting of single perovskite type layers of corner-sharing CoO_6-octahedra, Co(1), parallel to the *ac*-plane of the unit cell. These layers are connected by "layers" consisting of chains of corner-sharing CoO_4-tetrahedra, Co(2), running parallel to the *a*-axis. The unit cell comprises two such chains which are translated by ($\bar{b}/2 + \bar{c}/2$). The chains are related by centrosymmetry in space group *Pnma*. This space group allows all atoms to be placed in fully occupied positions (cf. Table 3). This structural model for $La_2Co_2O_5$ gave a quite reasonable fit to the observed data, see the calculated and difference profiles in Fig. 2. The not perfect fit to the PXD(SR) data is ascribed to a non-complete powder situation owing to the thin capillaries used.

TABLE 2 Unit cell data for $La_2Co_2O_5$ and reliability factors. Calculated standard deviations in parentheses.

		298 K	10 K
Crystal system		Orthorhombic	Orthorhombic
Space group		*Pnma*	*Pnma*
a, pm		544.45 (2)	543.4 (1)
b, pm		1586.89 (4)	1582.6 (3)
c, pm		569.22 (2)	568.7 (1)
V, 10^8(pm)^3		4.9180 (3)	4.891 (2)
Z		4	4
R_p (%) [a]	PXD(SR)	5.3	
	PND	5.6	14.3 [b]
R_{wp} (%) [a]	PXD(SR)	8.0	
	PND	7.3	22.0
R_{exp} (%)	PXD(SR)	5.7	
	PND	5.2	14.9
χ^2		1.97	2.17

[a] $R_p = 100(\Sigma|I_O-I_C|/\Sigma I_O)$, $R_{wp} = 100(\Sigma w(I_O-I_C)^2/\Sigma w I_O^2)^{-1/2}$ according to Ref. 8 (298 K) and Refs. 9, 10 (10 K).
[b] Combined refinement, crystallographic (R_N = 14.5%) and magnetic (R_M = 12.6%).

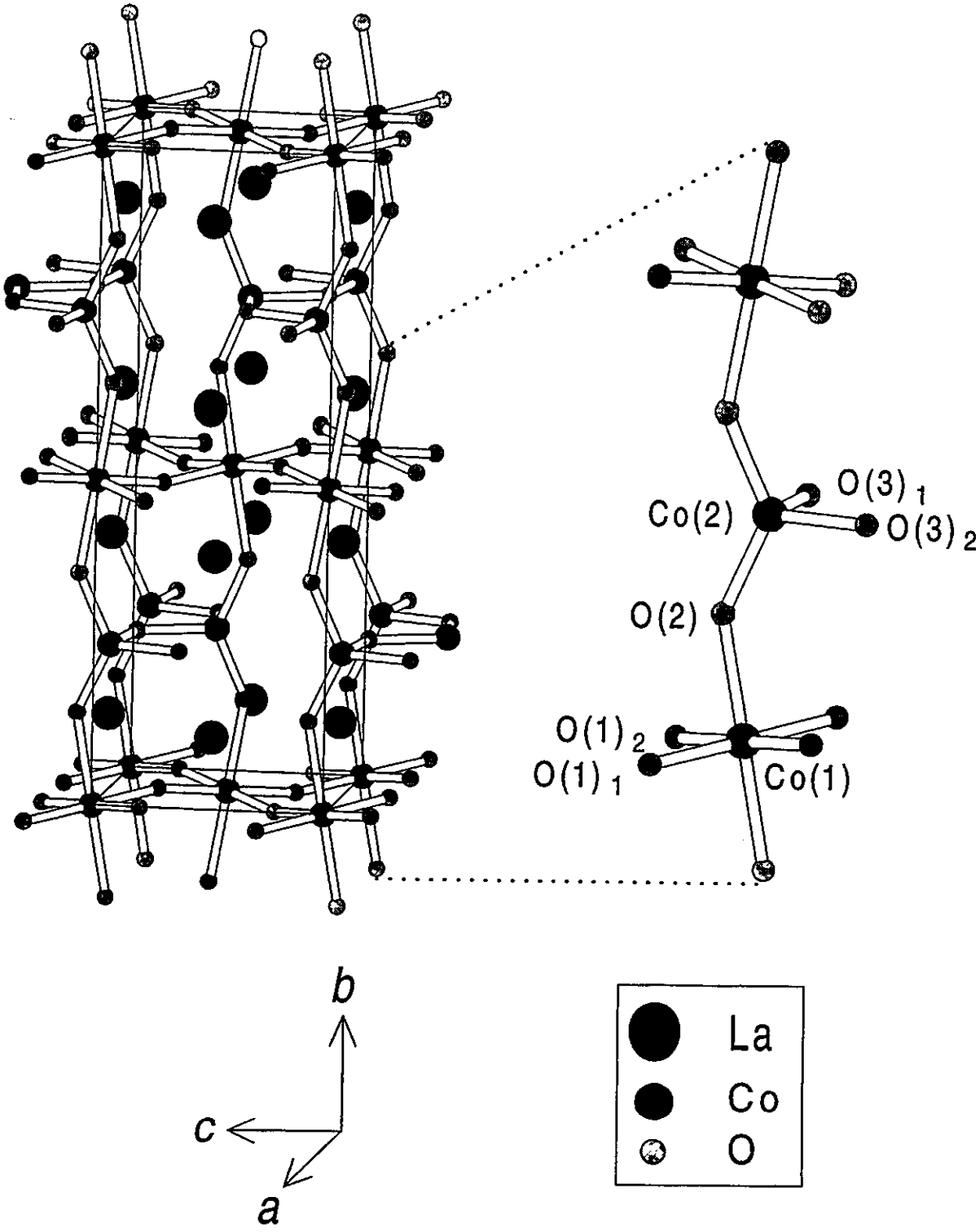

FIG. 1 Crystal structure of $La_2Co_2O_5$. Space group *Pnma*.

TABLE 3 Fractional atomic coordinates for $La_2Co_2O_5$ at 298 K. Calculated standard deviations in parentheses. Space group *Pnma*. Isotropic displacement factors (B_{iso} in $10^4 pm^2$): $B_{iso}(La) = 2.23\ (5)$, $B_{iso}(Co) = 0.4\ (1)$, $B_{iso}(O) = 1.43\ (8)$.

Atom	Wückoff site[a]	Coordinates		
		x	*y*	*z*
La(1)	*8d*	0.5002 (8)	0.11035 (9)	0.0148 (4)
Co(1)	*4a*	0	0	0
Co(2)	*4c*	0.972 (2)	0.25	0.936 (1)
O(1)	*8d*	0.242 (1)	0.9851 (3)	0.247 (1)
O(2)	*8d*	0.000 (1)	0.1418 (2)	0.0691 (6)
O(3)	*4c*	0.599 (1)	0.25	0.883 (1)

[a] *4a* (0,0,0), *4c* (*x*,¼,*z*), *8d* (*x*,*y*,*z*)

TABLE 4 Selected interatomic distances and bond angles for $La_2Co_2O_5$ at 298 K. Calculated standard deviations in parentheses. Atom numbers refer to Fig. 1.

	Distances (pm)			Angles (°)	
Octahedron:	Co(1) — $O(1)_1$	(×2)	194 (2)	$O(1)_1$—Co(1)—$O(1)_2$	93.4 (1)
	Co(1) — $O(1)_2$	(×2)	203 (1)	O(1)—Co(1)—O(2)	89.7 (5)
	Co(1) — O(2)	(×2)	228 (1)		
Tetrahedron:	Co(2) — O(2)	(×2)	188 (1)	O(2)—Co(2)—O(2)	131.6 (4)
	Co(2) — $O(3)_1$		205 (1)	$O(3)_1$—Co(2)—O(2)	98.1 (4)
	Co(2) — $O(3)_2$		195 (1)	$O(3)_2$—Co(2)—O(2)	110.2 (3)
				$O(3)_1$—Co(2)—$O(3)_2$	102.4 (4)

	Distances (pm)		Coordination
	La — O	240 - 279, 336 (1)	8 + 1

Polyhedra tilt angles (°):	Co(1)—O(2)—Co(2)	146.0 (3)
	Co(1)—O(1)—Co(1)	166.3 (2)
	Co(2)—O(3)—Co(2)	119.3 (4)

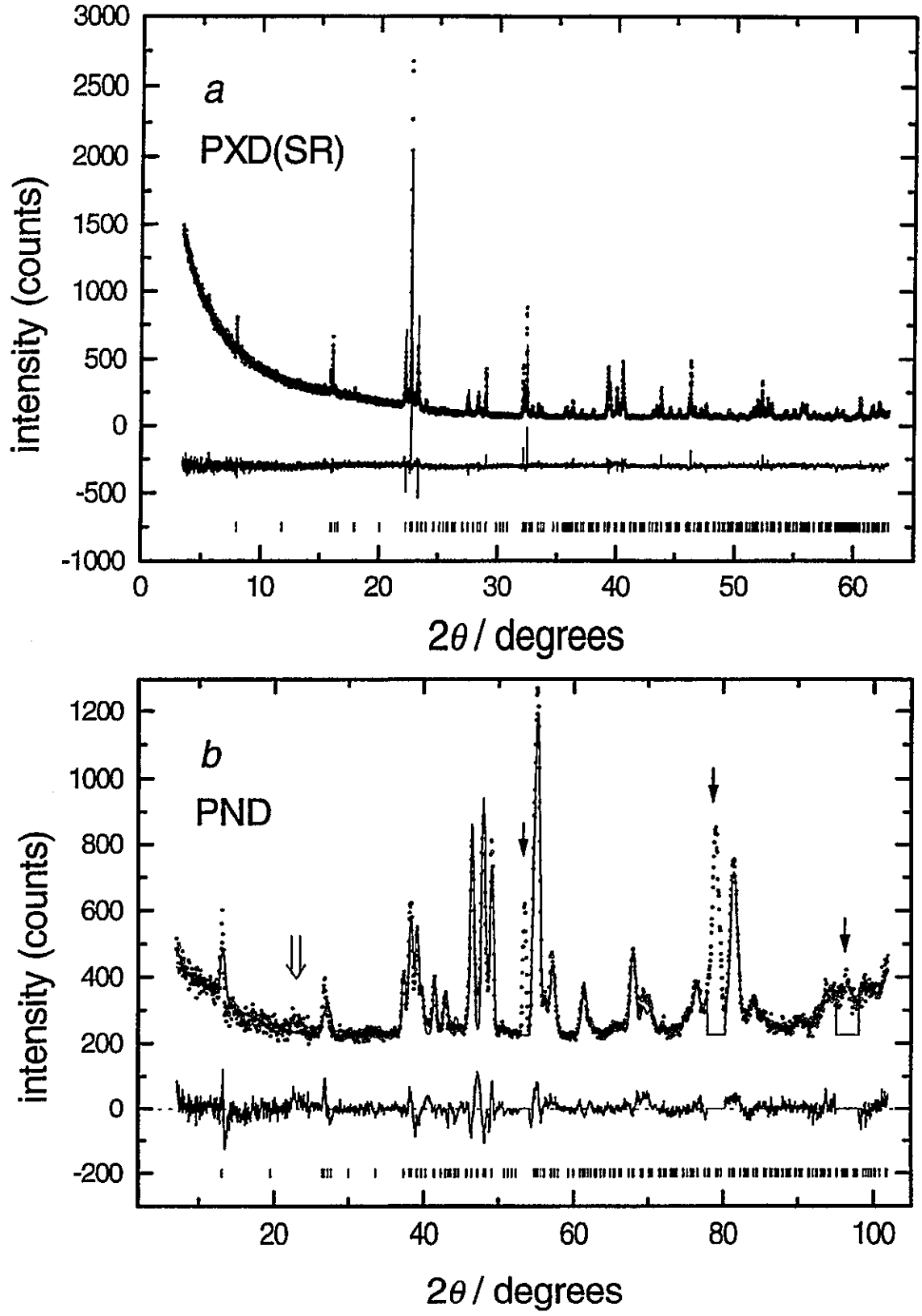

FIG. 2 a) Synchrotron PXD (λ = 109.803 pm) and b) PND (λ = 182.5 pm) profiles for $La_2Co_2O_5$ at 298 K. Experimental points marked by open circles, full line marks calculated profile, lower full line marks difference plot, vertical bars marks positions for Bragg reflections. Solid arrows in the PND pattern mark excluded reflections from the aluminum container, open arrow marks weak magnetic scattering.

In describing the structure for $La_2Co_2O_5$, two alternative body centered descriptions were examined which implies slightly different structural distortions and also atomic disorder. The first model refers to the space group *Imma* description of $Sr_2Fe_2O_5$ (12). This model requires Co(2) and O(3) to be randomly distributed over half occupied *8i* (x,¼,z) positions. However, this model gave no significant improvement of the *R*-factors (PXD(SR): $R_p = 5.3\%$, $R_{wp} = 7.9\%$. PND: $R_p = 5.6\%$, $R_{wp} = 7.4\%$). The possibility of fixing Co(2) and O(3) in fourfold positions *4e* (0,¼,z) can be excluded since it leads to severe distortions of the CoO_4-tetrahedra and a poor fit. The second model is based on space group *Ima2*. All atoms can be placed in fully occupied positions and satisfactory tetrahedral coordination of Co(2) is provided. However, the tetrahedral chains are not related by centrosymmetry, and more irregular octahedra are obtained, e.g. with a significant deviation from 180° of the O(2)—Co(1)—O(2) angle (176.2°). The model gave no significant improvement of the *R*-factors (PXD: $R_p = 5.4\%$, $R_{wp} = 8.0\%$. PND: $R_p = 5.7\%$, $R_{wp} = 7.3\%$). There is no doubt that $La_2Co_2O_5$ basically adopts the brownmillerite type structure. However, the rather equivalent fit obtained for the refinements according to the space groups *Pnma*, *Imma* and *Ima2* shows that there is still some ambiguity concerning the space group assignment.

The peak shape of the PXD(SR) data for $La_2Co_2O_5$ (FWHM = 0.049°) is compared to that for $LaCoO_3$ (FWHM = 0.028°) in Fig. 3. Clearly, the $La_2Co_2O_5$ sample which was prepared by low temperature reduction has significantly broader reflections than $LaCoO_3$, which was equilibrated at higher temperatures and used as precursor for the reduction. Similar peak broadening occurs for the related low temperature reduced phases $La_3Co_3O_8$ and $La_4Co_3O_9$ (5, 11). The peak broadening may stem from particle strain, which is related to the expansion of the crystal structure occuring upon reduction (see below), combined with possible disordered intergrowth of units of related phases $La_nCo_nO_{3n-1}$ with different oxygen content, i.e. $n > 2$. The apparent particle size distribution is constant as seen by scanning electron microscopy. However, peak broadening due to formation of microdomains on symmetry lowering cannot be ruled out. On the other hand, this is not the cause for peak broadening during reduction of $La_4Co_3O_{10}$ to $La_4Co_3O_9$ since no such symmetry lowering occurs.

A closer inspection of Fig. 1 shows that the perovskite type cationic arrangement is essentially retained in the reduced phase $La_2Co_2O_5$. The unit cell dimensions for orthorhombic $La_2Co_2O_5$ are compared with relevant dimensions for rhombohedral $LaCoO_3$ (13) in Table 5. On reducing $LaCoO_3$ to $La_2Co_2O_5$ there is a 9.8% expansion of the unit cell volume. For

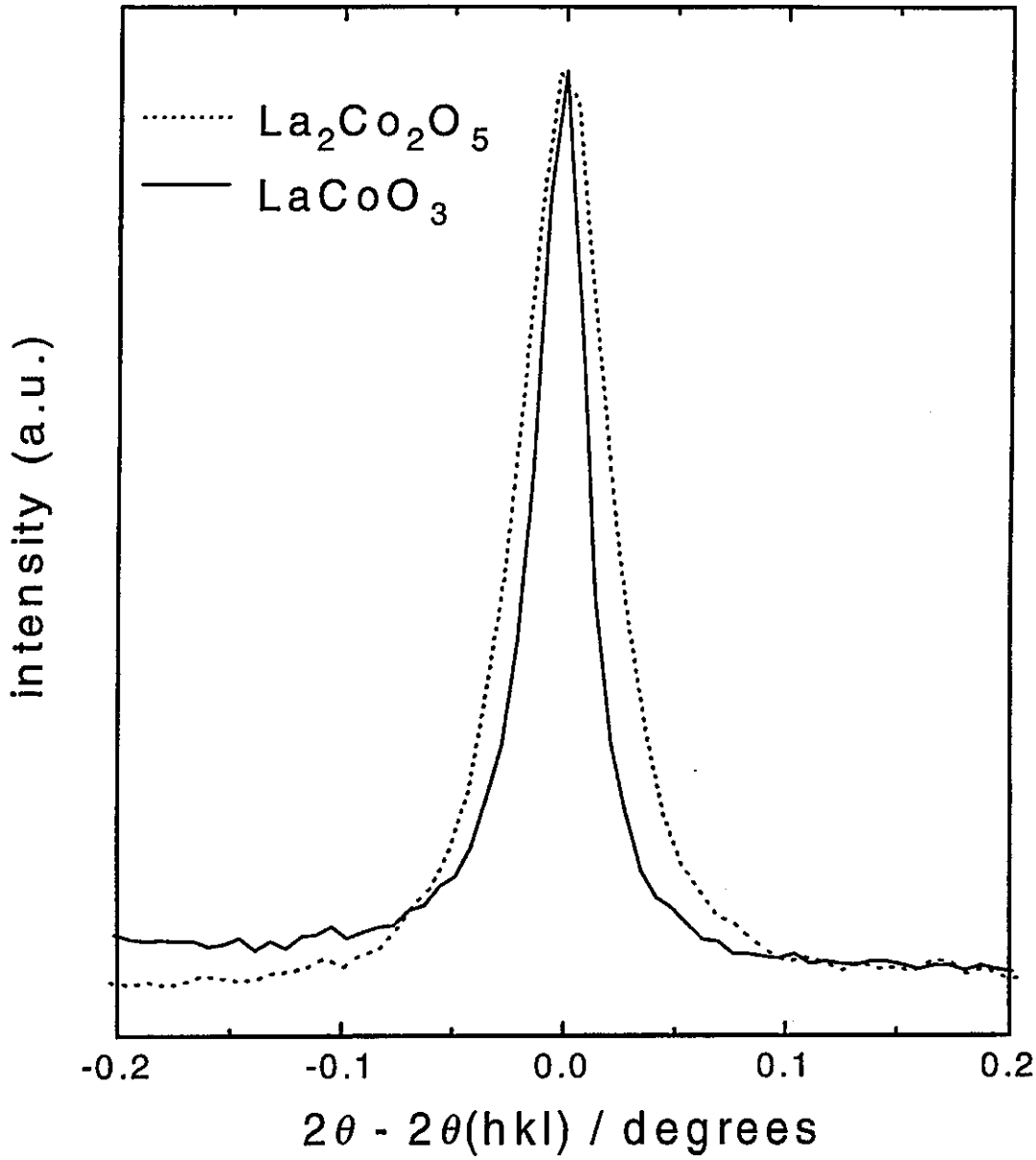

FIG. 3 Peak shape of reflections from PXD(SR) data for $La_2Co_2O_5$ (dotted line) and $LaCoO_3$ (full line). Reflections with Miller indices (200) for $La_2Co_2O_5$ at $d = 279.19$ pm and (104) for $LaCoO_3$ at $d = 268.70$ pm are plotted.

comparison, the expansion is 5.5% upon reduction of $LaCoO_3$ to $La_3Co_3O_8$. The main source for the volume expansion is the increased size of divalent, high-spin cobalt atoms, $Co^{II}(d^7)$, relative to trivalent, low-spin $Co^{III}(d^6)$. The small displacements of the Co(2) and the oxygen atoms together with the expansion of $\bar{c}$ reduce the distortions of the CoO_4-tetrahedra. At the same time considerable tilting of the CoO_6-octahedra occurs. Despite the displacements, the

tetrahedra are still distorted, especially along [010] as shown by the large O(2)—Co(2)—O(2) angle and the short Co(2)—O(2) interatomic distance (Table 4). Furthermore, the CoO_6-octahedra are significantly elongated along [010], and the nine fold coordination of oxygen around lanthanum is irregular.

Bond valences (14) for La and Co were calculated for $La_2Co_2O_5$ and all other ternary phases in the La-Co-O system for comparison, see Table 6. Common to all these phases is that the loss of oxygen due to reduction of Co^{III} to Co^{II}, is accompanied by a reduction of the coordination number of lanthanum from twelve to nine. The bond valences for trivalent lanthanum are significantly lower than expected for the phases $La_2Co_2O_5$, $La_4Co_3O_9$, and

TABLE 5 Comparison of unit cell dimensions for orthorhombic $La_2Co_2O_5$ (a, b, c) and rhombohedral $LaCoO_3$ (a_R, a_C, a_H).

$La_2Co_2O_5$		$LaCoO_3$[a]	
a (pm)	544.45	a_R (pm)	537.78
b (pm)	1586.89	$4a_C$ (pm)	1530.39
c (pm)	569.22	a_H (pm)	544.25
V (10^8pm^3)	4.918	V (10^8pm^3)	4.479

[a] Subscript R and H corresponds to the rhombohedral and hexagonal setting of the unit cell of $LaCoO_3$ (13), respectively. a_C refers to the Co-Co interatomic distance which corresponds to the a-axis of the cubic perovskite type unit cell.

TABLE 6 Calculated lanthanum and cobalt bond valences (v_i) for phases in the La-Co-O system.[a]

	Co^{II}-fraction	v_{Co} (tetrahedral)	v_{Co} (octahedral)	v_{La} (12 coord.)	v_{La} (9 coord.)	Ref.
$LaCoO_3$	0	---	3.21	3.17	---	13
$La_4Co_3O_{10}$	1/3	---	2.84, 2.92 3.02, 3.22	2.98, 3.03	2.98, 3.11	15
$La_3Co_3O_8$	2/3	1.92	2.44, 3.16	2.73	2.81, 3.03	5
$La_2Co_2O_5$	1	2.08	2.23	---	2.64	this work
$La_4Co_3O_9$	1	1.92	2.27	---	2.65, 2.75	11
La_2CoO_4	1	---	2.82	---	2.52	16

[a] $v_i = \Sigma\exp[(D_i - d_i)/0.37]$ (cf. Ref. 14), $D_{Co^{II}} = 1.692$, $D_{Co^{III}} = 1.700$, $D_{La^{III}} = 2.172$, d_i = experimentally determined interatomic distances.

La_2CoO_4, with solely divalent cobalt and nine coordinated La. The low lanthanum bond valences possibly indicate that nine fold coordination is unfavourable for La. The increasing (and more favourable with respect to valence) coordination for La in the Co^{III}-containing phases may act as an additional driving force for the oxidation reaction.

All the structural features discussed for $La_2Co_2O_5$ are common for several $A_2M_2O_5$ compounds with the brownmillerite structure, e.g. $Ca_2Fe_2O_5$ (2), $Sr_2Fe_2O_5$ (12), Sr_2CoFeO_5 (17), and $Sr_2In_2O_5$ (18). For $Sr_2Co_2O_5$ the brownmillerite structure is only obtained by quenching from high temperatures, whereas the low temperature crystal structure is rhombohedral. This deviating feature for $Sr_2Co_2O_5$ has been discussed to result from a larger size difference between the two cations (19-20). Whereas these and most other brownmillerite type phases are of the type $A^{II}_2M^{III}_2O_5$, the present phase is different with $La^{III}_2Co^{II}_2O_5$.

ii) Magnetic properties

The powder neutron diffraction study showed that additional magnetic reflections gain rapidly intensity on decreasing the temperature below ambient, see Fig. 4. There is still some observable (diffuse) magnetic scattering at 298 K, slightly above the background level, for the overlapping reflections (021) and (120), cf. open arrow in Fig. 2b. The antiferromagnetic ordering temperature T_N = 301 ± 5 K is estimated by extrapolation of the temperature dependence of the integrated intensity (Fig. 4) to the background level. All the magnetic reflections could be indexed on the crystallographic unit cell. Magnetic coupling for transition elements in the perovskite type oxides occurs typically through cation-anion-cation interactions, and the Co^{II}—O—Co^{II} interactions currently of interest are strongly antiferromagnetic (21). Assuming the main interactions to be antiferromagnetic in nature both for the tetrahedrally and octahedrally coordinated cobalt atoms, a number of possible models were tested out. The fit of the PND data to a model where the magnetic moments of all cobalt atoms are antiferromagnetically oriented relatively to the six nearest neighbouring cobalt atoms (G-type ordering) are given in Fig. 5. The obtained magnetic *R*-factor (R_M) is 12.6%. The antiferromagnetic ordering for $La_2Co_2O_5$ is shown in Fig. 6. The refined magnetic moments are $\mu_{oct.} = 3.0 \pm 0.1\mu_B$ for Co(1) and $\mu_{tetr.} = 2.5 \pm 0.1\mu_B$ for Co(2), both moments being oriented parallel to [101]. These values correspond fairly well to the expected value for high-spin $Co^{II}(d^7, S = 3/2)$. Similar strong G-type antiferromagnetic coupling is reported for several other brownmillerite phases: $Ca_2Fe_2O_5$ (22), Ca_2FeAlO_5 (23), $Sr_2Fe_2O_5$ (12), Sr_2CoFeO_5 (17), and $Sr_2Co_2O_5$ (24), all with $Fe^{III}(d^5)$ or $Co^{III}(d^6)$ in the high-spin state. For all the latter phases the magnetic moments are oriented parallel to either [100] or [001].

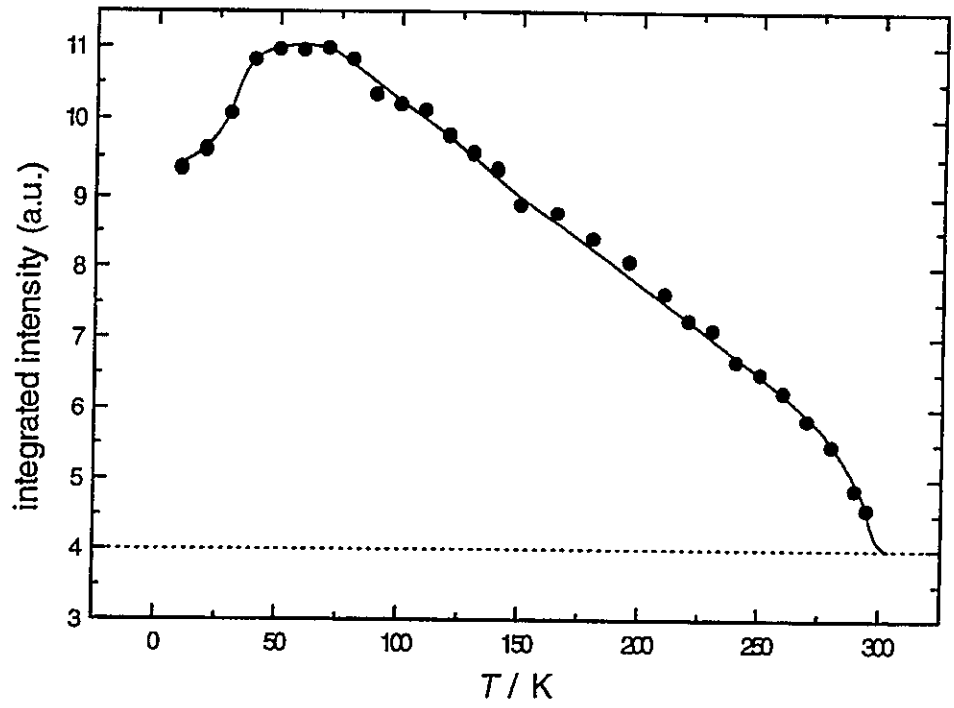

FIG. 4 Temperature dependence of the integrated intensity for the overlapping magnetic reflections (021) and (120). Dashed line represents the background level. Fully drawn line as guide to the eye.

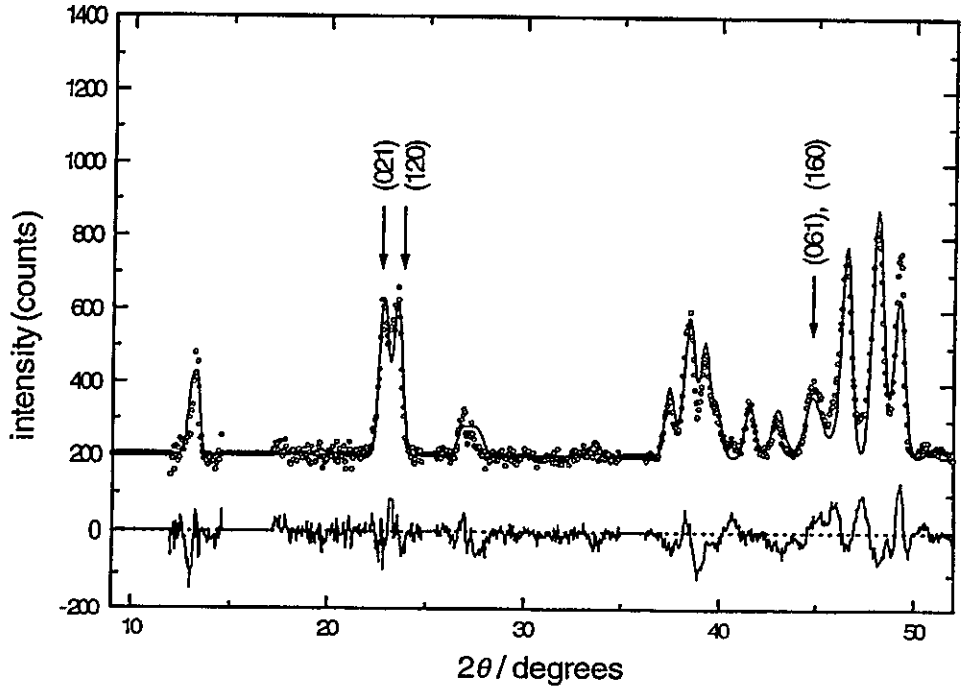

FIG. 5 Part of the observed PND profile for $La_2Co_2O_5$ at 10 K (λ = 182.5 pm). Miller indices for magnetic reflections are given. Experimental points marked by open circles, full line marks the calculated profile and lower full line marks the difference plot.

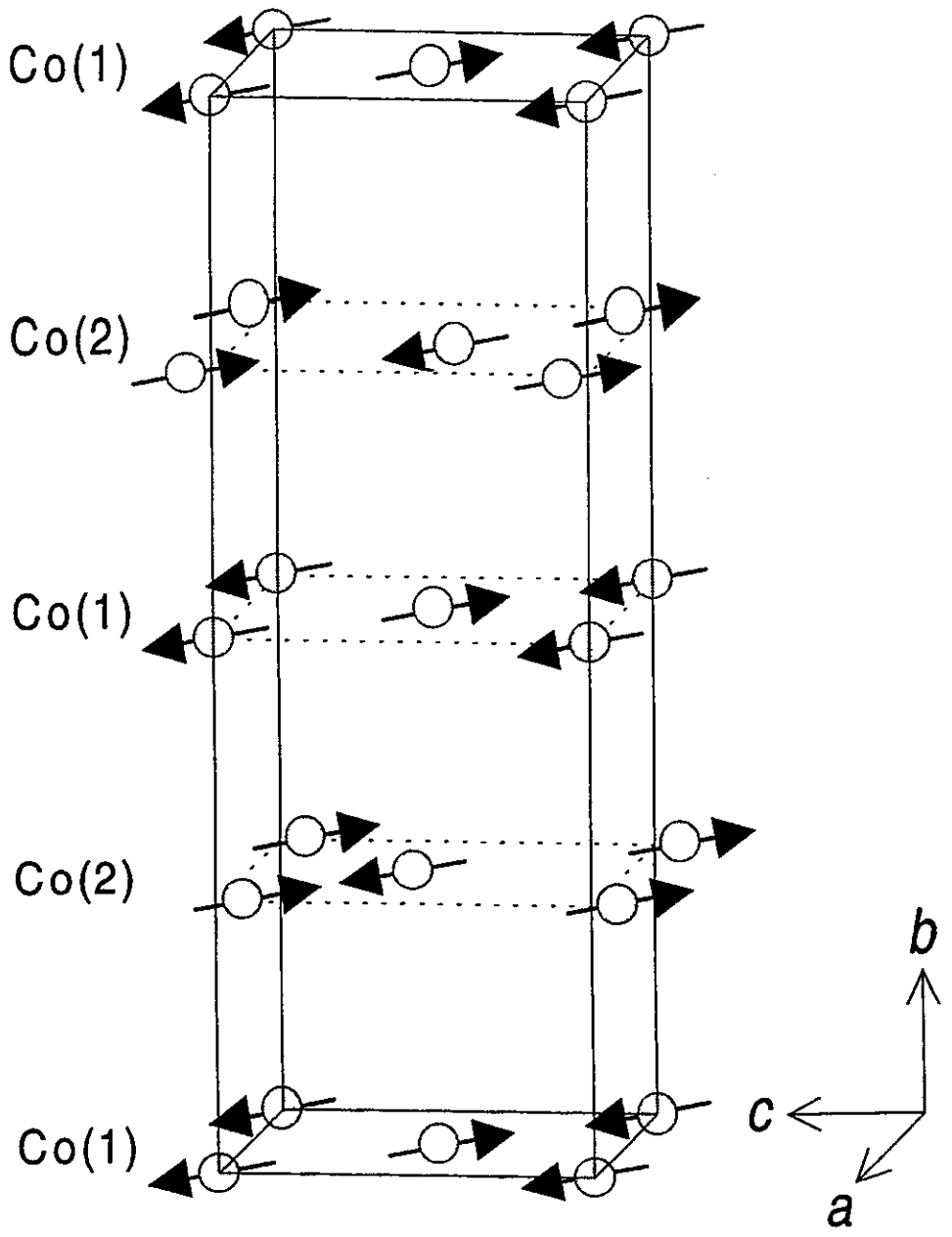

FIG. 6 Antiferromagnetic order in $La_2Co_2O_5$. Only Co-atoms shown.

The measured magnetization (M_g) of $La_2Co_2O_5$ (Fig. 7) shows several indications for a ferromagnetic impurity phase not detectable by PXD. The impurity is most probably minor amounts of metallic cobalt precipitated during the reduction. The magnetization is field dependent at all measured temperatures, and a small hysteresis is apparent in the $M_g(H)$ curve (Fig. 7b). Judged from the low magnetization, the ferromagnetic component is small and it is

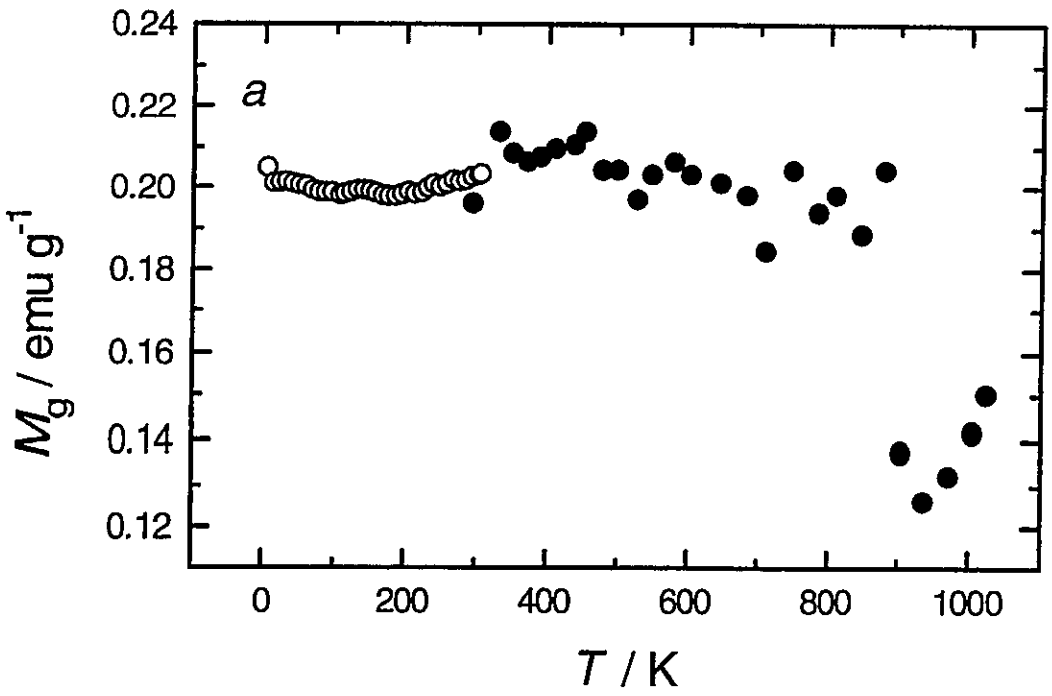

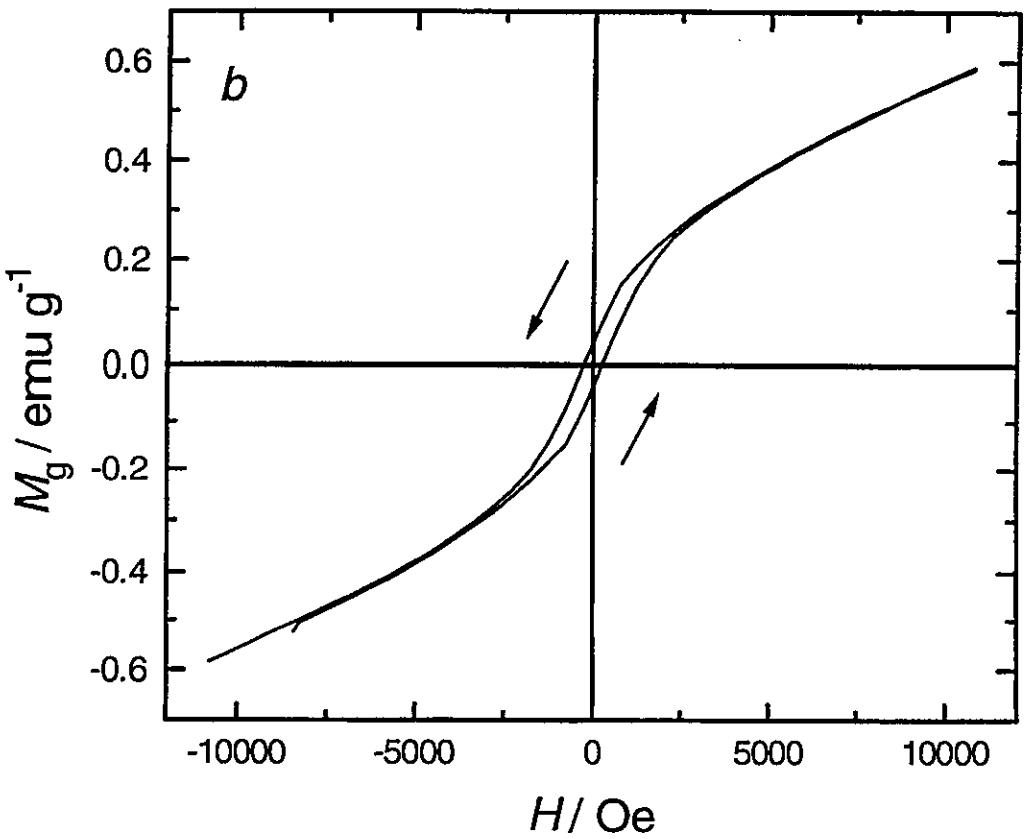

FIG. 7 a) Temperature dependence of the magnetization (M_g) for $La_2Co_2O_5$ between 5 and 1000 K (SQUID $T < 300$ K, Faraday $T > 300$ K) b) Field dependence of M_g for $La_2Co_2O_5$ at 5 K.

saturated in moderate fields. The present results are in accordance with the magnetization measurements of Sis *et al.* (25) on reduced samples of $LaCoO_{3-\delta}$. The magnetization is apparently temperature independent in low fields for $T < 880$ K (Fig. 7a), as typically observed for ferromagnetic materials at temperatures well below their disordering temperature [for bulk Co metal T_C is 1388 K (26)]. The abrupt drop in $M_g(T)$ at 880 K marks the onset of the decomposition of $La_2Co_2O_5$ into La_2CoO_4 and CoO. The decomposition was confirmed by PXD and differential thermal analysis (5). The magnetization shows poor reproducibility between different samples, which suggests inhomogenous distribution of the ferromagnetic impurity phase throughout the bulk sample. According to temperature programmed reductions of $LaCoO_3$ (27), CoO, and Co_3O_4 (28) the binary cobalt oxides can be reduced to metallic cobalt at a lower temperature than presently adopted during reduction (673 K), whereas higher temperatures are required for complete reduction of $La_2Co_2O_5$ to metallic cobalt and La_2O_3. The existence of binary cobalt oxides as precursor impurities for formation of Co(s) can not be ruled out (29). However, it appears also plausible that Co(s) is formed owing to surface or inhomogenous reduction, or simply by a minor excess of the reducing agent.

ACKNOWLEDGEMENT

This work has received financial support from the Research Council of Norway. The skilful assistance from project team at the Swiss-Norwegian Beam Line, ESRF is gratefully acknowledged. Contribution No 98.xx from the Swiss-Norwegian Beam Line at ESRF.

REFERENCES

1. C. N. R. Rao, J. Gopalakrishnan and K. Vidyasagar, *Indian J. Chem.* **23A**, 265 (1984)
2. J. Berggren, *Acta Chem. Scand.* **25**, 3616 (1971)
3. K. Vidyasagar, A. Reller, J. Gopalakrishnan and C. N. R. Rao, *J. Chem. Soc., Chem. Commun.* 7 (1985)
4. O. H. Hansteen, H. Fjellvåg and B. C. Hauback, *J. Solid State Chem.* submitted (Paper 3 of this thesis)
5. O. H. Hansteen, H. Fjellvåg and B. C. Hauback, *J. Mater. Chem.* submitted (Paper 1 of this thesis)
6. B. Gilbu, H. Fjellvåg and A. Kjekshus, *Acta Chem. Scand.* **48**, 37 (1994)
7. B. Noläng, *Program UNITCELL*, Department of Chemistry, Uppsala University, Sweden

8. A. C. Larson and R. B. Von Dreele, *Program GSAS, General Structure Analysis System,* LANSCE, MS-H 805, Los Alamos National Laboratory, Los Alamos, NM 87545, USA
9. A. W. Hewat, Harwell Report RRL 73/239 (1973)
10. H. M. Rietveld, *J. Appl. Crystallogr.* **2**, 65 (1969)
11. O. H. Hansteen, H. Fjellvåg and B. C. Hauback, *J. Mater. Chem.* submitted (Paper 4 of this thesis)
12. C. Greaves, A. J. Jacobson, B. C. Toefield and B. E. F. Fender, *Acta Cryst.* **31B**, 641 (1975)
13. G. Thornton, B. C. Toefield and A. H. Hewat, *J. Solid State Chem.* **61**, 301 (1986)
14. I. D. Brown and D. Altermatt, *Acta Cryst.* **41B**, 244 (1985)
15. H. Fjellvåg, O. H. Hansteen, B. C. Hauback, F. Fauth and P. Fischer, to be published
16. U. Lehmann and Hk. Müller-Buschbaum, *Z. Anorg. Allg. Chem.* **470**, 59 (1980)
17. P. D. Battle, T. C. Gibb and P. Lightfoot, *J. Solid State Chem.* **76**, 334 (1988)
18. R. von Schenck and Hk. Müller-Buschbaum, *Z. Anorg. Allg. Chem.* **395**, 280 (1973)
19. J. Rodriguez and J. M. Gonzalez-Calbet, *Mater. Res. Bull.* **21**, 429 (1986)
20. J. Rodriguez, J. M. Gonzalez-Calbet, J. C. Grenier, J. Pannatier and M. Anne, *Solid State Commun.* **62**, 231 (1987)
21. J. B. Goodenough, *Magnetism and the Chemical Bond*, John Wiley & Sons, New York (1963)
22. T. Takeda, Y. Yamaguchi, S.Tomoyoshi, M. Fukase, M. Sugimoto and H. Watanabe, *J. Phys. Soc. Jpn.* **24**, 446 (1968)
23. R. W. Grant, S. Geller, H. Wiedersich, U. Gonser and L. D. Fullmer, *J. Appl. Phys.* **39**, 1122 (1968)
24. T. Takeda, Y. Yamaguchi and H. Watanabe, *J. Phys. Soc. Jpn.* **33**, 970 (1972)
25. L. B. Sis, G. P. Wirtz and S. C. Sorenson, *J. Appl. Phys.* **44**, 5553 (1973)
26. R. V. Colvin and S. Arajs, *J. Phys. Chem. Solids* **26**, 435 (1965)
27. B. Gilbu Tilset, H. Fjellvåg and A. Kjekshus, *J. Solid State Chem.* **119**, 271 (1995)
28. P. Arnoldy and J. A. Moulijn, *J. Catal.* **93**, 38 (1985)
29. M. A. Señarís-Rodríguez and J. B. Goodenough, *J. Solid State Chem.* **116**, 224 (1995)